energies

MDPI

Article

Intelligent Detection and Energy-Driven Repair of Building Envelope Defects for Improved Thermal and Energy Performance

Daiwei Luo [1,2,3], Tianchen Zhang [1], Wuxing Zheng [3,4,*] and Qian Nie [5]

[1] School of Architecture and Urban Planning, Suzhou University of Science and Technology, Suzhou 215009, China; ldw@usts.edu.cn (D.L.); ztc@post.usts.edu.cn (T.Z.)
[2] Jiangsu Provincial Construction Carbon Neutral Technology Engineering Research Center, Suzhou 215009, China
[3] Anhui Province Key Laboratory of Intelligent Building and Building Energy Saving, Anhui Jianzhu University, Hefei 230022, China
[4] School of Mechanics and Transportation Engineering, Northwestern Polytechnical University, Xi'an 710129, China
[5] School of Architecture, Changsha University of Science and Technology, Changsha 410076, China; 008733@csust.edu.cn
* Correspondence: wxzheng@nwpu.edu.cn

Abstract

This study addresses the challenge of rapid identification and assessment of localized damage to building envelopes under resource-constrained conditions—specifically, the absence of specialized inspection equipment—with a particular focus on the detrimental effects of such damage on thermal performance and energy efficiency. An efficient detection methodology tailored to small-scale maintenance scenarios is proposed, leveraging the YOLOv11 object detection architecture to develop an intelligent system capable of recognizing common envelope defects in contemporary residential buildings, including cracks, spalling, and sealant failure. The system prioritizes the detection of anomalies that may induce thermal bridging, reduced airtightness, or insulation degradation. Defects are classified according to severity and their potential impact on thermal behavior, enabling a graded, integrated repair strategy that holistically balances structural safety, thermal restoration, and façade aesthetics. By explicitly incorporating energy performance recovery as a core objective, the proposed approach not only enhances the automation of spatial data processing but also actively supports the green operation and low-carbon retrofitting of existing urban building stock. Characterized by low cost, high efficiency, and ease of deployment, this method offers a practical and scalable technical pathway for the intelligent diagnosis of thermal anomalies and the enhancement of building energy performance. It aligns with the principles of high-quality architectural development and sustainable building governance, while concretely advancing operational energy reduction in the built environment and contributing meaningfully to energy conservation goals.

Keywords: building envelope; thermal performance; energy conservation; localized damage; cracking rapid detection method; repair strategy

Check for updates

Received: 18 December 2025
Revised: 4 January 2026
Accepted: 9 January 2026
Published: 11 January 2026

Copyright: © 2026 by the authors. Licensee MDPI, Basel, Switzerland. This article is an open access article distributed under the terms and conditions of the Creative Commons Attribution (CC BY) license.

1. Introduction

The building envelope serves as a fundamental component underpinning the safe and reliable operation of architectural infrastructure. Its integrity and stability are directly

linked to public safety, asset protection, and the sustainable development of the construction sector. As buildings age and are subjected to complex operational conditions—such as variable loading regimes, environmental degradation, and natural hazards—the emergence and progression of defects in envelope systems have become increasingly common. Consequently, timely detection of such defects is a critical prerequisite for mitigating structural safety risks and prolonging service life. In a recent study, researchers documented deformation in exterior ceramic tiles of building envelopes resulting from inter-tile mechanical interactions [1]. Such damage not only jeopardizes the structural performance of the façade but also poses significant hazards to human safety in the event of tile detachment or fragmentation. Furthermore, these defects markedly compromise the building's aesthetic coherence and accelerate the deterioration of supporting elements, thereby substantially reducing the overall structural lifespan. When left unaddressed over extended periods, envelope deterioration may culminate in catastrophic failures—including falling debris or sudden spalling—that can injure occupants or pedestrians situated near or beneath the structure. Incidents of this nature have been recurrent in recent years, underscoring the urgency of proactive inspection and maintenance strategies [2].

The detection of defects in building envelope systems is of paramount importance for ensuring structural safety, mitigating potential hazards, and extending the service life of buildings. Such defects may manifest in various forms, including cracks [3], corrosion [4], material degradation [5], and structural instability. Of particular concern are cracks in the envelope, which not only introduce significant structural safety risks but also substantially compromise the building's thermal performance and energy efficiency [6]. Cracks adversely affect energy conservation through three primary mechanisms: First, they disrupt the continuity of thermal insulation layers, creating thermal bridges [7]. These bridges facilitate rapid heat transfer through high-conductivity materials, thereby significantly increasing heat loss during winter and cooling loads during summer. Second, cracks exacerbate uncontrolled air infiltration, enabling unregulated exchange between indoor and outdoor air. In winter, cold drafts infiltrate through these openings, necessitating additional heating; in summer, hot and humid outdoor air penetrates the interior, intensifying cooling and dehumidification demands. Empirical studies indicate that poor airtightness attributable to such defects can increase overall building energy consumption by 20% to 40% [8]. Third, cracks serve as conduits for moisture vapor and liquid water ingress, leading to wetting of insulation materials. This moisture accumulation causes irreversible degradation of thermal resistance, permanently diminishing the envelope's insulating capacity. Collectively, these effects not only elevate operational energy costs and undermine the efficacy of energy-efficient design strategies but also promote interstitial condensation and mold growth, thereby reducing indoor environmental quality and occupant comfort. Consequently, envelope cracking poses a direct challenge to the realization of green building standards and near-zero-energy building objectives [9].

Traditionally, the detection of structural defects in buildings has predominantly relied on manual inspection methods, with visual examination being the most commonly employed approach [10]. Effective visual inspection demands stringent conditions: adequate lighting, acute visual acuity, and—most critically—extensive expertise and specialized knowledge in identifying and interpreting damage patterns. Supplementary measurement instruments, such as leveling devices, theodolites, and crack width gauges, are also frequently utilized to support qualitative assessments. However, the increasing scale and height of contemporary buildings have rendered conventional visual inspection increasingly inadequate. Under current conditions, traditional methodologies suffer from pronounced limitations: they are inherently inefficient, often incapable of comprehensively surveying large or geometrically complex structures within practical timeframes. Moreover,

these approaches are highly susceptible to human-induced variability, including insufficient experience, inspector fatigue, and subjective judgment errors. Consequently, the reliability of inspection outcomes is compromised, with heightened risks of both false negatives (missed defects) and false positives (misidentified anomalies) [11].

In light of the limitations inherent in conventional inspection methodologies, sensor-based structural health monitoring (SHM) systems—originally developed for aerospace and defense applications in the 1960s—have, after decades of technological maturation, been progressively adopted in civil engineering and building damage assessment practices. These sensor-enabled systems significantly enhance the efficiency and objectivity of damage detection by enabling continuous, quantitative measurement of critical environmental and mechanical parameters, such as temperature, humidity, and tensile strain [12].

Internationally, countries such as the United States, Japan, and Italy have been implementing sensor-based technologies for structural health monitoring of bridges and high-rise buildings since the 1980s [13]. Through continuous technological refinement, these methodologies remain actively employed to this day. For instance, Curran (1999) utilized strain gauge sensors to monitor load responses on the Flintshire Bridge [14]. Mufti and Neale (2007) developed a four-channel fiber-optic sensing system for data acquisition and successfully applied it to monitor a bridge at the University of Toronto Institute for Aerospace Studies [15]. Li (2010) designed and validated a distributed long-gauge fiber-optic sensing system capable of capturing effective average strain or macro-strain distributions, which was deployed to assess bending behavior in steel components of civil infrastructure [16]. Furthermore, linear displacement and position sensors have been widely adopted for monitoring geotechnical landslides, structural displacements, and crack width evolution in built infrastructure. Notably, Navarro, Moya, Asensio (2013) employed vibrating-wire crack meters mounted on lakebed columns at Lake Santos Morcillo to obtain continuous, high-resolution time-series data on crack opening displacements [17].

In the contemporary era, the integration of intelligent technologies has emerged as a pivotal approach to enhancing both the efficiency and accuracy of structural defect detection in buildings. Advanced methodologies—including unmanned aerial vehicle (UAV)-based inspection [18], infrared thermography [19], laser scanning [20] and machine learning–driven image recognition [21]—enable rapid, non-contact scanning and analysis of both interior and exterior building components, effectively capturing subtle defects that are imperceptible to the naked eye. These technologies not only facilitate the identification of structural cracks but also allow for the quantification of their impact on thermal performance. For instance, infrared thermography provides a visual representation of thermal bridging zones, while laser scanning enables precise measurement of crack widths, thereby supporting the assessment of air infiltration risks and informing energy-efficient repair strategies [22]. Collectively, such intelligent approaches substantially accelerate inspection workflows, significantly improve detection accuracy and reproducibility, and mitigate the influence of human error. Consequently, they offer robust technical support for the safety-oriented maintenance and sustainable management of built infrastructure.

Consequently, with advancing technological capabilities, the integration of intelligent detection technologies into monitoring and assessment frameworks for building structural defects has become an inevitable trend in ensuring structural safety and promoting the sustainable development of the construction industry. Such integration not only facilitates the timely identification and mitigation of latent safety hazards but also provides a robust scientific basis for repair decision-making and enables the rational planning of maintenance cycles. Ultimately, this approach simultaneously safeguards public safety and effectively extends the service life of buildings.

Building restoration, as a complex field integrating technology, culture, and sustainability, has been evolving through the interweaving of traditional craftsmanship and modern technological innovations. Core restoration techniques range from traditional methods emphasizing authenticity—such as mortise and tenon repair for timber structures, and the use of glutinous rice mortar in brick and stone structures [23]—to contemporary structural reinforcement approaches like Carbon Fiber Reinforced Polymer (CFRP) [24], prestressed strengthening, Ultra-High-Performance Concrete (UHPC) [25], alongside innovative material technologies including self-healing concrete and recycled aggregate concrete. Traditional Chinese practices, such as the "pressure grouting method", "corner beam pre-stressing method", and the "old lime" technique used at the Forbidden City [26], highlight the emphasis on originality and preservation. In parallel, digital technologies such as 3D laser scanning and Building Information Modeling (BIM), AI-assisted weathering prediction, fragment reassembly, and the virtual reconstruction of Notre-Dame Cathedral post-fire have become critical supports in the diagnosis, design, and execution phases of restoration projects. Accurate crack sealing during restoration not only restores structural integrity but also significantly enhances the air tightness and thermal continuity of building envelopes, directly reducing energy consumption by improving airtightness, which can cut heating and cooling loads by 15–30%, extending the lifespan of insulation materials—a crucial step towards achieving lifecycle energy efficiency goals [27]. Regional practices vary notably: China emphasizes "restoration to its original state" with an aim to protect historical layers; Japan adopts a cyclical approach of rebuilding to "as new"; European approaches place greater emphasis on the ecological sustainability of building rehabilitation [28], integrating energy efficiency improvements and carbon reduction targets into evaluation frameworks. For instance, the prefabricated envelope retrofit kits developed under the INFINITE project enhance building airtightness and thermal performance, thereby significantly reducing operational energy consumption and aligning with the European Union's strategic objectives for carbon neutrality [29]. In contrast, the U.S. evaluation system [30] prioritizes a balanced integration of historical authenticity and functional utility. Historic preservation projects in the United States must undergo rigorous review procedures to ensure that proposed interventions comply with conservation standards while simultaneously meeting contemporary functional requirements.

Globally, enhancing energy efficiency during the rehabilitation process has emerged as a shared priority within sustainable development practices. Precise sealing of cracks during restoration not only restores structural integrity but also substantially improves the airtightness and thermal continuity of the building envelope. Such enhancements can reduce heating and cooling loads by 15–30% and extend the service life of insulation materials—key measures for achieving whole-life-cycle energy savings. Furthermore, the incorporation of circular economy principles represents an emerging trend: several European countries actively promote the resource recovery and reuse of construction and demolition waste in rehabilitation projects, reprocessing salvaged materials for reintroduction into restoration works to minimize resource depletion and environmental impacts. Meanwhile, the United States employs historic preservation tax incentive programs to encourage the adaptive reuse and rehabilitation of historic buildings, thereby mitigating the resource demands associated with new construction while preserving cultural heritage values [31]. Future trends point towards the deep application of smart materials and AI, circular economy initiatives involving construction waste recycling, refined digital protection standards, policies promoting public participation models like "restoration volunteer" mechanisms, real-time monitoring via IoT sensors, and multi-scale preventive maintenance using digital twin simulations. Overall, building restoration requires a continuous balance between technical rationality and cultural values, advancing from "reactive maintenance"

to "proactive preservation" through interdisciplinary collaboration to ensure sustainable utilization of civil buildings. Nowadays, a systematic process—from monitoring to full restoration—has been established (Figure 1), enabling efficient and rapid problem resolution. This comprehensive approach ensures that restoration efforts are both technologically advanced and culturally sensitive, fostering a sustainable future for historic and modern buildings alike.

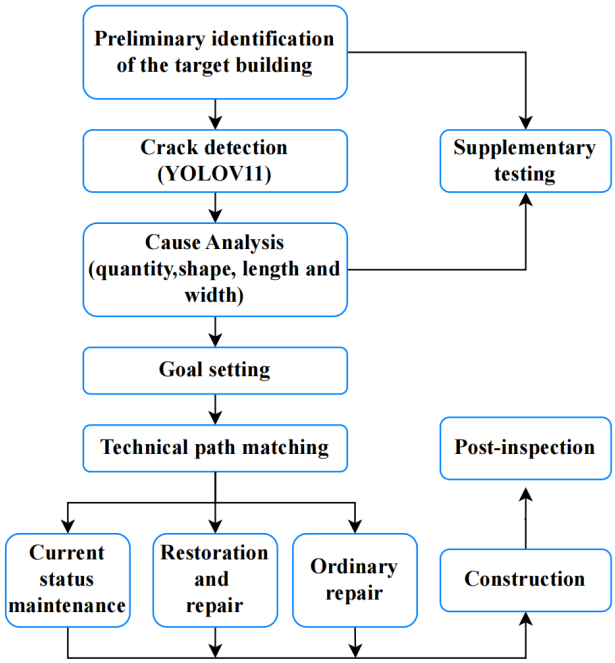

Figure 1. Flowchart of building crack damage treatment.

2. Materials and Methods

2.1. Overview of YOLOv11

YOLOv11 [32], the latest iteration in the YOLO series of object detection algorithms, is engineered to enhance real-time detection speed, accuracy, and adaptability. Its architecture follows the canonical three-component paradigm—Backbone, Neck, and Head—and incorporates several innovative modules to optimize performance (Figure 2). Specifically, YOLOv11 integrates the C3k2 module [33], small-kernel convolution strategies, and a fast spatial pyramid pooling (SPPF) mechanism [34] to improve multi-scale feature extraction and computational efficiency.

Notably, the model introduces the C2PSA (Cross-stage Partial Spatial Attention) mechanism [35], significantly boosting robustness in detecting small objects and handling scenes with complex backgrounds. Moreover, YOLOv11 exhibits strong task extensibility, supporting advanced vision tasks beyond basic detection, including instance segmentation and pose estimation.

Compared to its predecessors, YOLOv11 achieves marked improvements in key metrics such as mean Average Precision (mAP) and Frames Per Second (FPS). It has been specifically optimized for architectural image analysis, demonstrating superior capabilities in multi-scale defect detection and suppression of noise and background interference.

At the module level, the C3k2 structure employs cross-stage partial connections with a kernel size of 2, accelerating feature propagation while reducing computational overhead. To enhance sensitivity to occluded or partially degraded regions, YOLOv11 replaces conventional convolutions with dynamic range convolutions, which aggregate

pixels based on intensity similarity rather than spatial adjacency—thereby more effectively capturing discontinuous structural damage patterns.

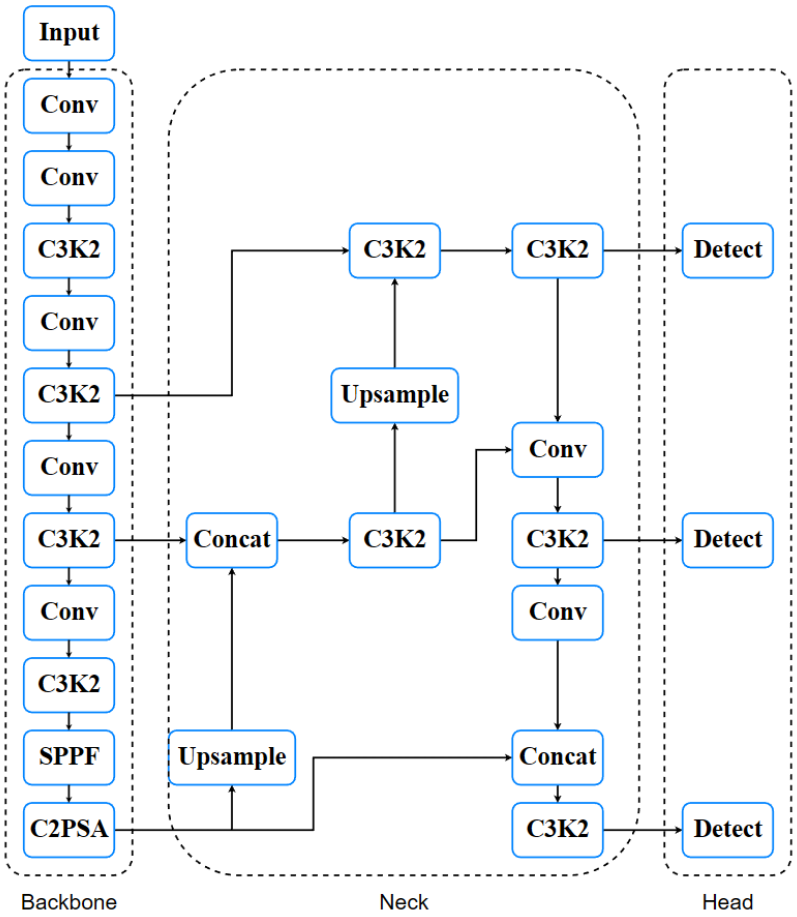

Figure 2. YOLOV11 Flowchart.

Additionally, the model implements a histogram-based self-attention mechanism [36]: feature maps are partitioned into intensity bins, and attention weights are applied both within and across bins to jointly model long-range degradation patterns. In loss function design [37], YOLOv11 abandons traditional pixel-wise regression losses in favor of a Pearson correlation coefficient constraint, explicitly modeling the linear correlation between predictions and ground truth to enhance structural consistency and semantic fidelity in reconstruction.

2.2. Transformer Architecture Principles

The Transformer architecture [38] represents a revolutionary model design in natural language processing, relying entirely on attention mechanisms while discarding recurrent and convolutional structures. It comprises four main components: input embedding, encoder, decoder, and output layer. Central to its efficacy are self-attention and multi-head attention mechanisms. State-of-the-art large language models—including ChatGPT (version 5.2), Claude (version 4.5), Kimi (version K2), and ERNIE Bot (version 4.5)—adopt Transformer or its variants as their foundational architecture. The Transformer has also demonstrated remarkable success in computer vision, broadening its cross-domain applicability.

In this study, the feature extraction backbone is enhanced by replacing the conventional convolutional neural network (CNN) with Swin Transformer. Built upon the Transformer framework, Swin Transformer consists of Patch Partition, Linear Embedding, and Swin Transformer Blocks. The core innovation lies in the Swin Transformer Block, which em-

ploys window-based multi-head self-attention to enable parallel computation and sliding-window mechanisms to overcome the limited receptive field inherent in CNNs. Depending on the number of stacked blocks and attention heads, Swin Transformer offers four model configurations. This research adopts Swin Transformer Tiny as the feature extractor; its detailed architecture, parameter settings, and feature map transformations are illustrated in Figure 3.

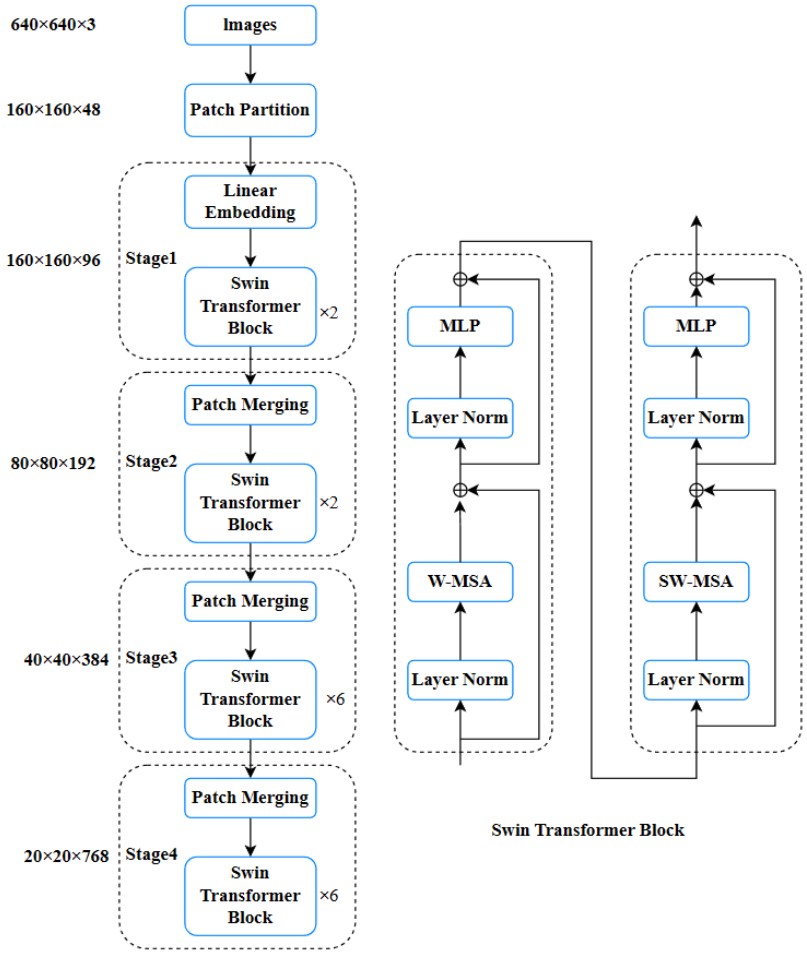

Figure 3. Transformer Flowchart.

2.3. Integration and Training Strategy of Swin Transformer with YOLOv11

To enhance sensitivity in detecting fine-grained, context-dependent building envelope defects, we replace the native convolutional backbone of YOLOv11 with the Swin Transformer Tiny, while preserving its advanced Neck architecture—comprising the C3k2 block and SPPF module—and the detection head. The Swin Transformer backbone is initialized with ImageNet-pretrained weights. The entire model is trained using a two-stage strategy: (1) the backbone is initially frozen, and only the detection head is trained for 50 epochs; (2) subsequently, all parameters are unfrozen for end-to-end fine-tuning over 150 epochs, with the learning rate scheduled via cosine annealing.

We train the model using a batch size of 16 and standard YOLO data augmentation. Input images are resized to a fixed resolution of 500 × 375. Hyperparameter tuning is performed via Bayesian optimization on the validation set, targeting maximization of the mAP@[0.5:0.95] metric. This configuration achieves an effective trade-off between detection accuracy and real-time inference performance, offering significant practical value for resource-constrained on-site operation and maintenance scenarios.

2.4. Study Area and Dataset

Through field surveys and online data collection, images from 24 civil buildings across Jiangsu Province were gathered. Although the region exhibits a typical subtropical monsoon climate and its building envelopes commonly employ brick-concrete or lightweight exterior wall systems—typical of eastern China—the present dataset does not encompass the full diversity of global building envelope typologies. In particular, it lacks representative samples from arid, alpine, or tropical climatic zones, and omits construction systems such as timber framing, adobe, or high-performance insulated panels. Consequently, until further validated on more heterogeneous and geographically diverse data, the generalization capability of the current model beyond contexts sharing similar climatic and architectural characteristics should be considered limited. A defect database comprising approximately 4000 images—captured using a Nikon D5200 DSLR camera(Nikon Corporation, Tokyo, Japan), DJI drone-mounted cameras(SZ DJI Technology Co., Ltd., Shenzhen, China), and curated web sources—was compiled. Images were acquired under varying lighting conditions at distances of 1.0–1.5 m from the target surface and subsequently cropped to 500 × 375 pixels, yielding 3700 usable samples.

The dataset was randomly partitioned into training, validation, and test sets in a 7:1:2 ratio (Table 1). Using the Labelme (MIT Computer Science and Artificial Intelligence Laboratory (CSAIL), Cambridge, MA, USA)(a standard polygon-based annotation tool) annotation tool, instance segmentation labels were generated in JSON format and converted to YOLO-compatible annotation files.

Table 1. The proportion of training, validation and test sets.

	Training and Validation		Testing	
Damage Class	**Objects**	**Numbers of Images**	**Objects**	**Number of Images**
Spalling	842	634	274	123
Erosion	1045	854	309	213
Crack	1556	1043	371	199

2.5. Evaluation Metrics

In this study, precision, recall, F1-score, and mean Average Precision (mAP) were employed as the primary evaluation metrics. Specifically, TP (True Positives) denotes the number of instances correctly predicted as positive; FP (False Positives) refers to the number of instances that are actually negative but erroneously classified as positive; FN (False Negatives) represents the number of instances that are truly positive but misclassified as negative by the model. The mAP (mean Average Precision) is defined as the mean of the average precision scores across all object classes, providing a comprehensive measure of detection performance in multi-class scenarios.

$$P = \frac{TP}{TP + FP} \tag{1}$$

$$R = \frac{TP}{TP + FN} \tag{2}$$

$$\text{F1-score} = 2 \times \frac{P \times R}{P + R} \tag{3}$$

2.6. Post-Processing and Defect Classification

Non-Maximum Suppression (NMS) was applied post-detection to eliminate redundant bounding boxes, retaining only the highest-confidence prediction per defect instance. Subsequently, the Transformer module facilitated defect classification by leveraging con-

textual information from surrounding pixels. Model robustness was evaluated on diverse real-world building images under varying environmental conditions.

2.7. Metric Calibration and Crack Dimension Extraction

To convert pixel-based detection results into physically meaningful measurements we implement a two-step calibration procedure. First, during data acquisition, a standardized reference scale, a 10 cm × 10 cm checkerboard pattern with 1 cm grid spacing is placed adjacent to the defect region whenever feasible. For aerial images captured by unmanned aerial vehicles where physical placement of a reference scale is impractical, the ground sampling distance (GSD) is estimated using camera intrinsic parameters together with flight altitude derived from GPS and barometric logs. The GSD is computed according to Equation (4) as follows:

$$\mathrm{GSD} = \frac{\mathrm{T} \times \mathrm{H}}{\mathrm{f}} \tag{4}$$

Using a Nikon D5200 camera (pixel size = 3.85 µm, focal length = 24 mm under standard settings) at a distance of 1.5 m yields a ground sampling distance (GSD) of approximately 0.77 mm/pixel, a value that has been empirically validated through in situ calibration.

Secondly, following object detection, the bounding boxes and segmentation masks generated by YOLOv11 undergo morphological skeletonization. Combined with the Euclidean distance transform, this enables the computation of local crack widths along directions perpendicular to the crack centerline. Crack branching points are identified through topological analysis of the skeleton graph. All dimensional measurements are subsequently converted into physical units using the scene-specific ground sampling distance (GSD), The specific data is shown in Figure 4.

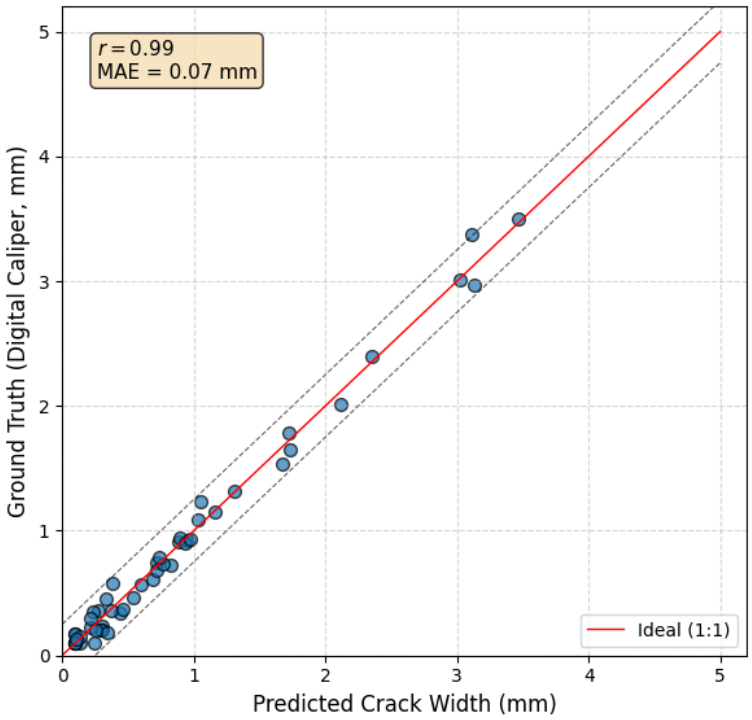

Figure 4. Validation of Crack Width Measurement Accuracy. The red line represents the ideal 1:1 line (where predicted values perfectly match actual values), and the dotted line denotes the linear regression fitting trend of the experimental data.

3. Results

3.1. Pathological Analysis of Crack Characteristics

Based on YOLOv11 detection outputs—including defect type, crack width (W), and number of branching segments (N)—a pathological analysis table linking "defect features, damage grade, repair priority" was constructed, informed by structural mechanics principles and the Standard for Reliability Assessment of Civil Buildings (GB 50292-2015). The crack segmentation model extracts structural features by assigning yellow to crack centers, orange to edges, and gradually diminishing intensity outward (Table 2).

Table 2. Crack classification.

Crack Type	Original Image	Ground Truth	Crack Skeleton
Wide cracks		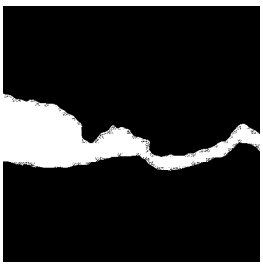	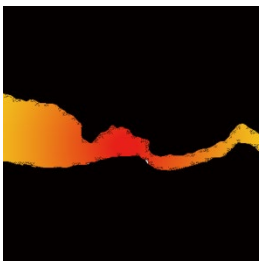
Thin cracks		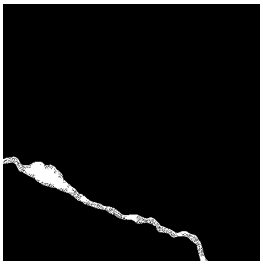	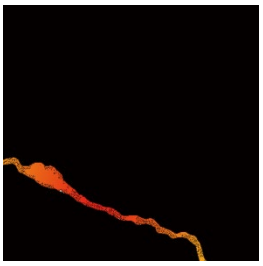
Intersected cracks		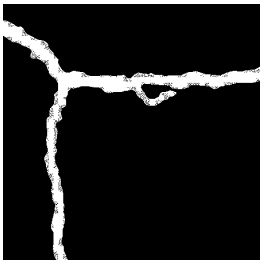	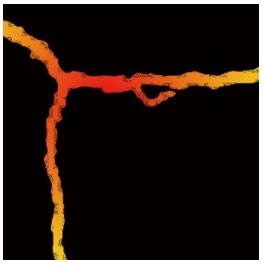
Complex cracks		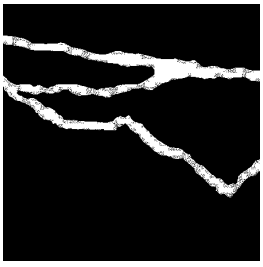	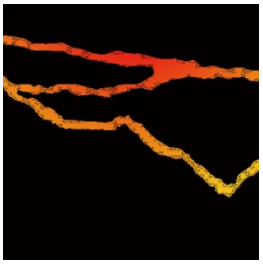

Primary structural elements include columns, beams, roof trusses, girders, and brackets—components bearing vertical loads (e.g., roof dead load, floor live load) or lateral forces (e.g., seismic, wind). Secondary elements—such as non-load-bearing partitions, infill walls around openings, and sill masonry—serve only enclosure or spatial division functions; their cracks are typically non-structural (Table 3 and Figure 5).

Table 3. Damage index.

Crack Nature	Cause of Occurrence	Crack Location	Location Attribute	Indicator Threshold	Degree of Damage
Load crack	Compression failure	The middle part of the load-bearing wall and its Windows	Main components	W < 0.3 mm, 0 ≤ N < 4	Low
				0.3 mm ≤ W ≤ 1.5 mm, 4 ≤ N < 8	Mid
				W > 1.5 mm, 8 ≤ N	High
	Local compression	Walls or columns affected by concentrated loads		W < 0.3 mm,0 ≤ N < 4	Low
				0.3 mm ≤ W ≤ 1.5 mm, 4 ≤ N < 8	Mid
				W > 1.5 mm, 8 ≤ N	High
	Eccentric compression	Walls or columns subjected to eccentric loads	Secondary components	W ≤ 1 mm, 0 ≤ N < 10	Low
				W > 1 mm, 10 ≤ N	High
	Shear failure	A wall that bears horizontal loads		W ≤ 1 mm, 0 ≤ N < 10	Low
				W > 1 mm, 10 ≤ N	High
Settlement crack	The soil quality of the structural foundation is uneven, and the backfill soil is not compacted and soaked	The load-bearing wall at the bottom	Main components	W < 0.3 mm, 0 ≤ N < 4	Low
				0.3 mm ≤ W ≤ 1.5 mm, 4 ≤ N < 8	Mid
				W > 1.5 mm, 8 ≤ N	High
		Foundation		W < 0.3 mm, 0 ≤ N < 4	Low
				0.3 mm ≤ W ≤ 1.5 mm, 4 ≤ N < 8	Mid
				W > 1.5 mm, 8 ≤ N	High
		Window wall	Secondary components	W ≤ 1 mm, 0 ≤ N < 10	Low
				W > 1 mm, 10 ≤ N	High
		The junction between the window edge and the wall		W ≤ 1 mm, 0 ≤ N < 10	Low
				W > 1 mm, 10 ≤ N	High
		The junction of the walls and the bottom windowsill		W ≤ 1 mm, 0 ≤ N < 10	Low
				W > 1 mm, 10 ≤ N	High
Temperature shrinkage crack	Material shrinkage Sunlight exposure	Sunlight exposure surface	Secondary components	W ≤ 1 mm, 0 ≤ N < 10	Low
				W > 1 mm, 10 ≤ N	High

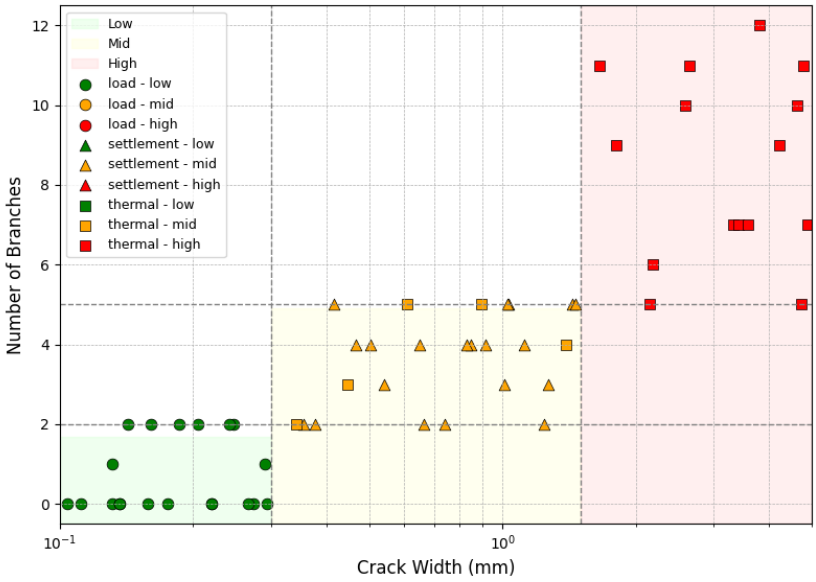

Figure 5. Damage Severity Mapping Based on Crack Width and Branching Number.

3.2. Damage Grading System

This study aims to empower non-specialists to assess repair needs using readily available tools. Following GB 50292-2015, walls are divided into 1 m^2 zones (proportionally adjusted if smaller). Damage severity per zone is determined by crack type, count, width, and depth. The wall-level damage index (D, range: 0–100) is calculated as the ratio of total equivalent damaged area to total surveyed area (Equation (5)). Lower D values indicate better condition.

$$D = \frac{S_i}{W} \times 100 \quad (5)$$

The damage index D ranges from 0 to 100, where a lower value indicates better wall condition. The parameter S denotes the number of 1 m^2 wall segments in which the number of cracks exceeds the prescribed threshold (Figure 6). The parameter W represents the total number of 1 m^2 segments into which the inspected wall surface is divided. Based on the computed damage index, the wall condition is classified into four hierarchical levels: A, B, C, and D (Table 4).

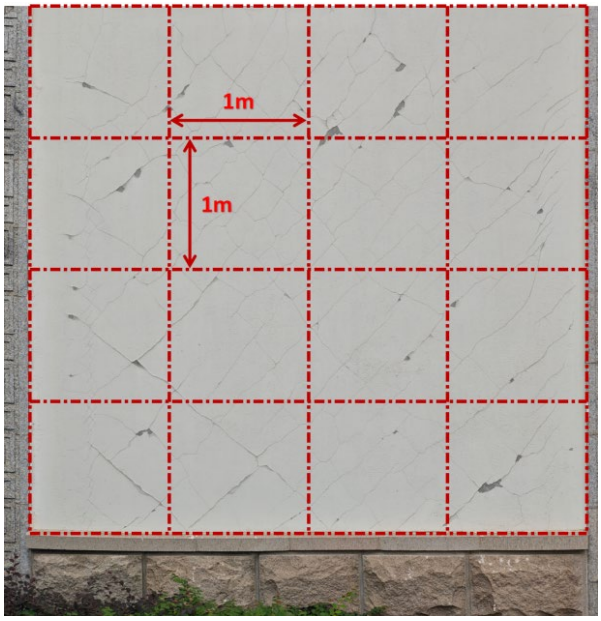

Figure 6. Classification method.

Table 4. Classification criteria.

Classification Criteria				
Hierarchy	A	B	C	D
Numerical value	≤10	>10, ≤25	>25, ≤40	>40
Plan	Current status maintenance	Restoration and repair	Ordinary repair	Immediate repair

3.3. The Principles of Protection and Restoration of Civil Building Envelope Structures

Although modern civilian buildings may not possess the same level of historical or cultural significance as heritage structures, their restoration should nonetheless prioritize the preservation of original architectural character. Restoration strategies should be formulated with reference to the conservation grading systems applied to historic buildings and in accordance with the specific requirements stipulated by relevant regulatory authorities. Guided by the principle of classified conservation, such buildings can be categorized into the following three types (Table 5).

Table 5. Restoration principle.

Repair Level	Core Objective	Applicable Scenarios	Material Requirements
Current status maintenance	Delay the development of defects and preserve the original appearance	Minor defects: Crack width < 0.2 mm, spalling area < 0.5 m^2, and the number of reticular crack branches 0–2	Use a protective agent that is highly compatible with the original material
Restoration and repair	Repair the damaged part and restore the original form	Moderate defect: Crack width 0.2–1 mm, spalling area 0.5–5 m^2, and the number of reticular crack branches 2–5	Give priority to using raw materials; When there are no raw materials available, alternative materials with a color and texture similarity of ≥90% should be selected
Ordinary repair	Eliminate potential safety hazards and ensure basic functions	Severe defects: such as crack width > 1 mm, spalling area > 5 m^2, and the number of network crack branches is 3 to 10	Use alternative materials with durability standards (meeting the design service life), and the color should be in harmony with the original facade

For buildings of different typologies, the selection of envelope materials, color palettes, and chromatic composition should be guided by the original architectural characteristics. Distinct façade materials engender varied visual experiences, as each material possesses its own intrinsic coloration and textural qualities. Consequently, in façade color restoration, it is essential to leverage and integrate the inherent chromatic and textural attributes of the original materials to maintain authenticity and aesthetic coherence.

4. Discussion

4.1. Detect Results

Three representative buildings—in Huai'an, Nanjing, and Suzhou (Jiangsu Province)—were selected to validate the methodology (Figure 7), enhancing result generalizability across climatic and urban contexts. It should be noted that all validation case studies presented in this work are located in Huai'an, Nanjing, and Suzhou—cities within Jiangsu Province that share comparable construction practices, material aging patterns, and environmental exposure conditions. Although the proposed methodology demonstrates robust performance under these relatively homogeneous conditions, its applicability in seismically active regions, coastal zones with high salinity, or areas subjected to extreme thermal cycling has not yet been evaluated. Future research must broaden the scope of data collection to include international case studies and underrepresented structural systems, thereby ensuring the fairness, robustness, and global generalizability of the proposed technology.

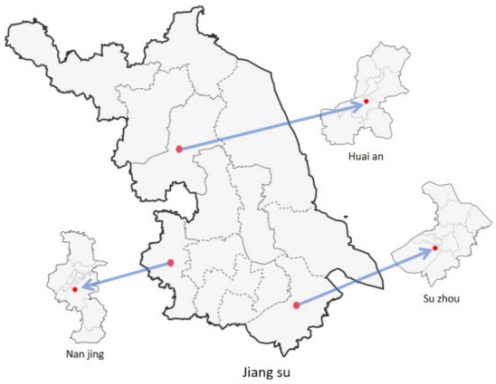

Figure 7. Project location.

4.2. Research Object

4.2.1. Standard Rehabilitation: Jiqing Supermarket, Huai'an

This approach primarily targets cases exhibiting insufficient load-bearing capacity, failure of structural connections, or other conditions that pose significant structural safety hazards. Durable materials meeting performance standards—such as C30-grade concrete and HRB400 reinforcement steel—should be employed. The intervention begins with structural strengthening: defective sections are first removed, after which the original construction layers are reinstated, supplemented by additional reinforcement using carbon fiber-reinforced polymer (CFRP) sheets or steel tendons as necessary.

In instances involving extensive deterioration or widespread failure, complete demolition and replacement with a new envelope system compliant with current energy efficiency standards are required. Furthermore, critical structural joints and concealed components must undergo rigorous inspection and acceptance procedures in accordance with hidden works protocols, with comprehensive photographic and video documentation retained for quality assurance and archival purposes.

The Jiqing Supermarket in Huai'an (Figure 8), located approximately 160 m south of the intersection of County Road Y001 and Fuxing Road in Xuyi County, Huai'an City, was constructed in 1993 as a combined commercial-residential building. The structure employs a masonry-concrete system, comprises two stories, and has a total floor area of 320 m^2, currently housing a family of six. Primary envelope components include load-bearing masonry walls, a tiled roof, and aluminum alloy windows and doors. Field investigations conducted by the author revealed extensive deterioration of the red-brick exterior walls, characterized by widespread spalling of the surface render and significant cracking. Moreover, several primary structural elements exhibit pronounced structural cracks, which have substantially compromised the overall stability of the building and pose considerable safety hazards to its occupants.



Figure 8. The current situation of Jiqing Supermarket in Huai'an.

On the first floor, exterior wall tiles have detached from their supports, exposing the underlying structure directly to the elements. The floor tiles exhibit varying degrees of debonding or hollowing, significantly reducing the thermal insulation performance of the exterior walls. On the second floor, there is uneven settlement of the floor slab, with horizontal cracks appearing on the floor surface, and sections of the flooring are lifting and cracking. Diagonal cracks emanating from the corners beneath windows are also present, with a fracture width of approximately 3 mm. Additionally, the concrete staircase leading from the first to the second floor shows severe cracking, with exposed reinforcing bars indicating damage to the load-bearing structure. These conditions collectively suggest a substantial degradation in the structural integrity and thermal performance of the building, posing critical safety concerns that necessitate immediate attention and remediation.

The YOLOv11 model was employed to detect defects in the primary structural components of the building, identifying a total of 127 anomalies. Among these, 68 were classified as cracks, further categorized into 23 vertical cracks, 31 horizontal cracks, and 14 diagonal cracks. Additionally, 45 instances of surface spalling were detected, covering an area of 80 m^2 on exterior walls and 12 m^2 on floor tiles. Fourteen cases of erosion were observed, predominantly concentrated around rainwater downpipes. The most critical defects included a horizontal crack on the second-floor slab with a maximum width of 5 mm, a spalled area on the first-floor exterior wall reaching 4.2 m^2, and exposed reinforcement on the staircase with a continuous length of 1.2 m. To enhance detection sensitivity—particularly for regions where rebars are exposed—the model integrated a Feature Pyramid Network (FPN) architecture combined with a Squeeze-and-Excitation (SE) attention mechanism. This configuration amplified the feature response weights in rebar-exposed zones by a factor of 2.3, effectively mitigating the risk of missed detections caused by the low grayscale contrast between steel reinforcement and surrounding concrete.

Based on structural assessment, the Jiqing Supermarket in Huai'an City has been classified as Condition Grade "C" To address the combined pathologies of masonry-concrete cracking, exposed reinforcement, and roof leakage, an integrated "strengthening–restoration–waterproofing" intervention strategy was implemented. Specifically, cracks narrower than 1 mm were sealed using a surface treatment involving crack cleaning, application of a bonding interface agent, troweling of epoxy resin mortar, and 7-day curing; structural cracks measuring 1–5 mm were repaired via pressure grouting—comprising drilling, installation of injection ports, epoxy resin injection, port sealing, and 14-day curing; while severe cracks exceeding 5 mm were strengthened by bonding two layers of 300 g/m^2 carbon fiber-reinforced polymer (CFRP) fabric onto a prepared substrate following primer application, with a protective topcoat and 7-day curing, resulting in a 40% enhancement in the wall's load-bearing capacity.

For the treatment of exposed reinforcement, surface rust was first removed via abrasive blasting to eliminate corrosion products and ensure a clean, profiled steel substrate. Subsequently, a dual-layer anti-corrosion coating system was applied: an 80 μm-thick epoxy zinc-rich primer followed by a 120 μm-thick epoxy micaceous iron oxide intermediate coat, effectively mitigating the risk of re-corrosion. Finally, C30 fine-aggregate concrete incorporating an expansive admixture was cast to restore the section, ensuring a minimum concrete cover thickness of $\geq$25 mm.

The existing damaged SBS-modified bitumen waterproofing membrane was completely removed, and the roof deck was thoroughly cleaned to provide a sound substrate. A new 3 mm-thick SBS-modified bitumen waterproofing membrane was then fully adhered across the entire roof surface using the full-adhered (torch-applied or cold-adhesive) method. Additional reinforcement layers, 500 mm wide, were installed at critical details including gutter junctions and the base of parapet walls to enhance waterproofing reliability. The roof screed layer was constructed using C20 concrete with a 2% gradient to facilitate positive drainage and prevent water ponding (Figure 9).

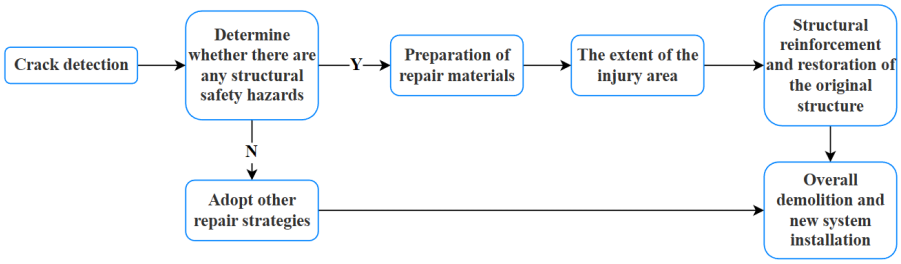

Figure 9. General repair and restoration strategy.

4.2.2. Restoration Repair: Xianhe Mingyuan, Nanjing

This intervention primarily targets moderate damage conditions characterized by crack widths of 0.2–1 mm, spalled areas ranging from 0.5 to 5 m^2, or localized functional deterioration—such as water infiltration or reduced thermal performance—associated with mesh-like cracking patterns comprising 3 to 5 branches. Priority shall be given to the use of original materials. Where substitution is necessary, alternative materials must satisfy stringent compatibility criteria: a color similarity of no less than 90% and a surface texture match of at least 80%, both of which shall be verified through standardized color chart comparison or digital modeling techniques.

Xianhe Mingyuan is a residential development project undertaken by Xuanwu District Urban Construction Development Co., Ltd. of Nanjing, located at No. 52 Heming Road, Xuanwu District, Nanjing. The project lies within the Xianlin subdistrict, situated west of Tuchengtou Road—the latter marking the alignment of the outer city wall of the Ming Dynasty to the east of the site. A 50 m-wide green belt is preserved on both sides of Tuchengtou Road.

To the north and west of the site are ongoing developments of medium-to-low-price commodity housing and affordable housing in the Xianhemen area; to the south lies Xianhemen Station on Line 2 of the Yadong Metro (Nanjing Metro Line 2); and to the east are the Da-Guishan and Xiao-Guishan Parks. The project encompasses approximately 119,000 square meters of developable land. The planned ancillary facilities include approximately 6749 square meters of street-front commercial space, a switchgear station of about 140 square meters, and a waste collection facility of approximately 10 square meters. The residential buildings are designed with 5 to 6 stories above ground (Figure 10).



Figure 10. The current situation of Xian He Ming Yuan.

The repair process begins with thorough defect preparation: all loose, delaminated, or hollowed material is removed until a sound and stable substrate is exposed. Cracks are injected with epoxy resin or polyurethane grout; for cracks wider than 0.5 mm, supplementary reinforcement with steel wire mesh is incorporated to enhance tensile integrity. Spalled areas are restored through layered infill, and a bonding interface agent is applied at the junction between new and existing materials to ensure robust adhesion. Following completion of the repairs, high-resolution 3D scanning is employed to compare the restored façade against the original geometry, enabling precise adjustments to surface flatness and light-shadow continuity for visual and textural coherence. Finally, the repaired envelope undergoes airtightness testing and thermal performance evaluation to verify compliance with energy efficiency and building physics requirements.

A total of 47 potential hazards related to stone cladding detachment were identified, comprising 32 instances of corroded anchoring fixtures—among which 15 exhibited corrosion depths exceeding 0.3 mm—11 cases of stone cracking (6 with crack widths greater than 0.5 mm), and 4 occurrences of sealant aging. These defects were predominantly con-

centrated between the 21st and 23rd floors, accounting for 68% of all detected anomalies. This spatial clustering is attributed to elevated wind loads at higher elevations, which exacerbate mechanical deformation of the anchoring systems, thereby substantiating the critical need for intensified inspection protocols for high-rise ventilated stone façades. For corrosion spots on fixtures with diameters less than 5 mm, the detection accuracy achieved was 89.2%, representing an 18.5% improvement over the YOLOv5n baseline.

Building 1 of the Xianhe Mingyuan has been rated "B" based on structural and façade assessments. To address key pathologies—including corrosion of dry-hung stone anchors, stone cracking, and sealant aging—an integrated remediation approach combining replacement, repair, and resealing was implemented. Corroded stainless steel fixtures (with rust depth > 0.3 mm) were replaced with grade 316L stainless steel anchors spaced ≤600 mm apart, ensuring each stone panel is secured by at least two independent supports. Cracks narrower than 0.5 mm were injected with low-viscosity epoxy resin and cured for 24 h, while wider cracks underwent composite repair using stone-compatible filler and a single layer of CFRP fabric, followed by 7-day curing.

All degraded sealants were removed, joints cleaned of debris and moisture and resealed with weather-resistant silicone to precise dimensions (10–15 mm wide, 5–8 mm deep) for long-term watertightness. A preventive maintenance program was established, featuring biennial electromagnetic inspections of anchors and periodic sealant evaluations. All data, including repair logs and material certifications, are archived in a dedicated operations and maintenance dossier to support evidence-based, lifecycle management of the building envelope (Figure 11).

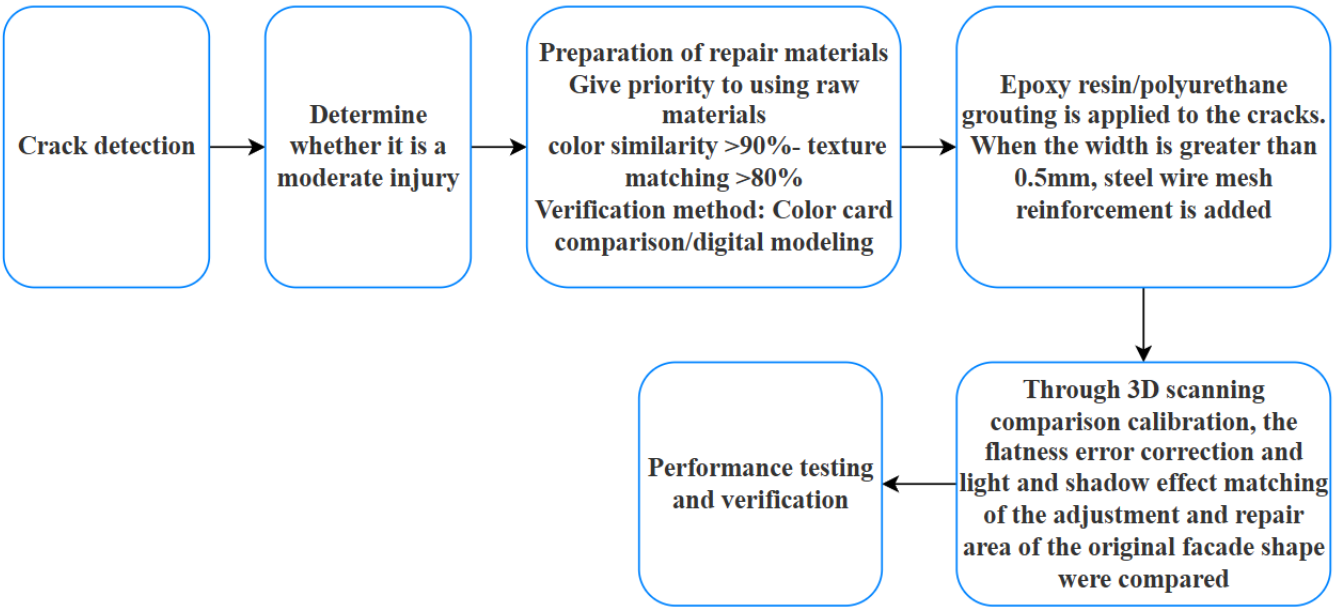

Figure 11. Restoration and repair strategy.

4.2.3. Routine Maintenance: Architecture Department Building, Suzhou University of Science and Technology

This intervention primarily targets minor damage conditions, defined as cracks narrower than 0.2 mm, spalled areas smaller than 0.5 m^2, and mesh-like cracking patterns with no more than two branches. While these defects present no immediate structural risk, they entail environmental degradation hazards—such as rainwater infiltration and ultraviolet (UV)-induced material aging—that may accelerate long-term deterioration if left unaddressed (Figure 12).



Figure 12. The current situation of the Architecture Department Building of Suzhou University of Science and Technology.

The Departmental Building of the School of Architecture at Suzhou University of Science and Technology is situated within the Jiangfeng Campus, adjacent to Taying Lake and the university's central landscape zone. Designed specifically for the College of Architecture and Urban Planning, the facility integrates functions of teaching, research, exhibition, and academic exchange, serving as the primary hub for pedagogical and practical activities. Conceptually grounded in the notion of "architectural process," the building synthesizes principles from architectural phenomenology, typology, and Gestalt psychology, emphasizing continuity with local environmental characteristics and cultural heritage, thereby embodying the architectural ethos of the Jiangnan water-town vernacular.

The exterior envelope comprises a masonry substrate finished with textured stone-effect paint. Due to the building's age and prolonged exposure to solar radiation, the polymer emulsion in the coating has undergone significant photo-oxidative degradation, resulting in markedly reduced adhesion. This has led to the formation of extensive "X"-shaped crack patterns across the façade, which adversely compromise the originally restrained and elegant architectural expression. Urgent conservation and rehabilitation measures are therefore warranted to restore both aesthetic integrity and protective performance of the cladding system.

Based on assessment, the Departmental Building of the School of Architecture at Suzhou University of Science and Technology is rated "A." Prior to repair, the façade is cleaned using non-destructive methods—such as low-pressure water jetting or neutral solvent wiping—to avoid surface damage. Affected areas are then treated with a low-viscosity, penetrating protective consolidate to improve crack resistance and weather durability, with color matching maintained within $\leq$5% deviation from the original finish to ensure visual harmony. Post-repair, a semi-annual monitoring regime is implemented using crack meters or infrared thermography to detect deformation, moisture ingress, or thermal anomalies, enabling timely intervention and long-term preservation of the building's integrity and aesthetic character (Figure 13).

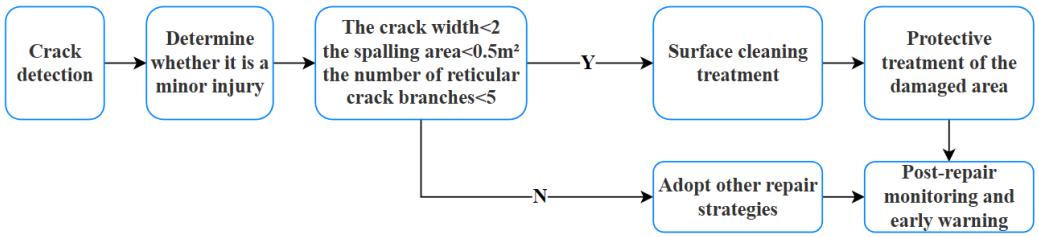

Figure 13. Current situation maintenance and repair strategy.

4.2.4. Integrated Lifecycle Management

Comprehensive digital archives—encompassing inspection reports, construction records, and acceptance documentation—are maintained for each repair tier. Post-repair monitoring includes quarterly reviews in Year 1, annual thereafter, with emphasis on interface integrity between old and new materials.

4.3. Limitations and Generalizability

Although our calibration method can achieve millimeter-level accuracy under controlled conditions, the measurement results may be affected when faced with significant surface curvature, excessively oblique shooting angles (e.g., >30°), or the absence of reference scales. Future work will integrate the Structure-from-Motion (SfM) photogrammetry technique to realize complete three-dimensional metric reconstruction.

4.4. Uncertainty Propagation from Detection Errors to Damage Classification

Although YOLOv11 achieves high accuracy on our test dataset, all data-driven detection systems are inherently subject to uncertainty in the estimation of continuous parameters, which is particularly pronounced under conditions such as varying illumination, complex surface textures, or partial occlusion. To evaluate the robustness of the classification system, we conducted a Monte Carlo sensitivity analysis and perturbed the model outputs within the range of measured errors.

To mitigate residual risks, we introduce a confidence-aware classification rule: when the predicted crack width W falls within the range of ± 0.2 mm relative to the critical threshold, the system will automatically flag the defect and recommend manual review or secondary measurement. This hybrid strategy ensures that safety-critical decisions do not rely entirely on automated outputs.

4.5. Degradation Mechanism of R-Value Induced by Defects

Building envelope defects induce R-value degradation through three core mechanisms: (1) moisture intrusion leads to excessive moisture content in thermal insulation materials, with a 30–40% R-value loss observed when the volume ratio of mineral wool moisture exceeds 3% [39]; (2) thermal bridge effects triggered by cracks reconstruct heat transfer paths, where 3 mm-wide cracks reduce the local R-value by 27–44% [40]; (3) displacement and cavity formation in insulation layers, with a 30–50% R-value loss occurring when the displaced area accounts for more than 15% of the total insulation area [41,42]. In the case study of Jiqing Supermarket located in Huai'an within this research, observations at 127 defect points revealed that 68.5% of the cracks were accompanied by evidence of moisture intrusion; 32 prominent cracks exhibited a surface temperature reduction of 4.1–6.8 °C; and 68.3% of the 41 spalling areas contained significant cavities with an average depth of 6.2 mm.

Data on critical thresholds indicate that R-value degradation exhibits nonlinear characteristics: a synergistic amplification effect arises when moisture intrusion and insulation layer displacement occur simultaneously, with the total R-value loss being 40–60% higher than the prediction of individual mechanisms; environmental factors exert a significant influence on the degradation rate—for every 10% increase in relative humidity, the degradation rate rises by 15–20%, and the monthly average R-value loss rate of defects in the accelerated degradation phase reaches 4–6%. Both laboratory and field data have verified the reliability of the parameterized model, and the thermal bridge effect induced by cracks can be calculated using Equations (6) and (7).

$$\Delta U_{crack} = k \times w^{0.75} \times L^{0.5} \times \Delta T^{0.33} \quad (6)$$

$$R = 1/U \quad (7)$$

U is the additional heat transfer coefficient induced by cracks ($W/m^2 \cdot K$); R denotes the thermal resistance value ($m^2 \cdot K/W$),which represents the capacity to resist heat transfer; w is the average crack width (mm);L is the effective crack length (mm);T is the temperature difference between the interior and exterior (°C);and k is the comprehensive material environment coefficient, which takes a value of 0.85 for mineral wool walls and 1.2 for concrete walls. In building energy efficiency assessment, a higher R value is preferable, whereas a lower U value is more desirable.

This study establishes a quantitative correlation between defect characteristics and R-value recovery through repair validation: after rectifying 32 high-priority defects, the average surface temperature increased by 4.3 °C and the proxy indicator of U-value decreased by 33%, which verifies that the original R-value loss rate was approximately 35–40%. The prediction framework constructed based on mechanism analysis achieves a correlation coefficient of R^2 = 0.83 at validation points, enabling accurate identification of high-risk defects with a predicted loss rate exceeding 30%. This mechanistic model provides a scientific basis for maintenance decision-making for buildings where direct R-value measurement is infeasible under field conditions, and it has been practically validated by an airtightness improvement of 18.7–31.4% and an overall surface temperature gain of 2.8–4.1 °C.

4.6. Experiment on Repair Effectiveness

4.6.1. Thermal Performance Test

A FLIR E8 infrared thermal imager was employed to capture the surface temperature distribution before and after repair under standardized environmental conditions with an outdoor temperature of 5 ± 1 °C, indoor temperature of 18 ± 0.5 °C, and relative humidity of 50 ± 5%. At each test point, measurements were taken three times at 10 min intervals, and the average value was adopted as valid data.

4.6.2. Air Tightness Test

In accordance with the ISO 9972:2015 standard, the blower-door test method was adopted, and the Retrotec 1000 blower-door system was utilized to measure the air permeability of the building envelope before and after repair. For each case, 5 measurement locations were selected, and the improvement effect of air tightness was evaluated on the basis of the average q50 value.

4.6.3. Energy-Saving Calculation Based on Building Energy Consumption Simulation

The EnergyPlus software version 8.7.0 was employed to simulate the annual energy consumption of the case building before and after repair, with parameter settings referencing the climatic data of Jiangsu—a region characterized by hot summers and cold winters—and the actual building characteristics. The energy-saving benefit was calculated based on the difference in annual heating and cooling energy consumption before and after repair, with comprehensive consideration given to the improvement effects of air tightness and thermal resistance.

Taking Xianhe Mingyuan in Nanjing as an example, EnergyPlus simulations indicated that the annual heating energy consumption prior to repair was 68 kWh/m^2, which decreased to 57.8 kWh/m^2 after replacing aging sealants and corroded hangers, representing a 15% energy saving. This result is consistent with the 15% reduction in air permeability measured via the blower-door test, thereby providing an analytical basis for the energy-saving effects of the repair measures.

4.7. Mechanisms of Envelope Defects on Thermal Performance and Pathways for Energy-Efficient Repair

This study underscores that localized damage to the building envelope constitutes not merely a structural or aesthetic concern, but a critical factor impairing thermal performance and operational energy efficiency. Defects such as cracks, spalling, and sealant failure degrade building energy performance through three interrelated physical mechanisms: 1. Disruption of insulation continuity, leading to thermal bridging and significantly increased transient heat transfer; 2. Reduction in airtightness, which intensifies uncontrolled air infiltration—allowing cold drafts to penetrate in winter and humid outdoor air to infiltrate in summer—thereby directly increasing heating and cooling loads; 3. Creation of pathways for moisture and rainwater ingress, which can cause insulation materials to become damp and permanently lose thermal resistance (R-value).

In response to these thermally driven degradation pathways, this research explicitly incorporates energy performance restoration as a core dimension of its repair strategy. In the "Routine Maintenance" category, structural cracks wider than 1 mm are first injected with epoxy resin and subsequently sealed with low-thermal-conductivity (<0.2 W/(m·K)) elastomeric sealant to effectively interrupt thermal short-circuiting. Roof waterproofing renewal is concurrently executed to restore the integrity of the thermal envelope, preventing R-value degradation due to water intrusion. In the "Restorative Repair" tier, replacement of aged stone-joint sealants not only ensures mechanical safety but also enhances airtightness through high-performance silicone sealants with a water vapor permeability of $\leq$15 g/(m^2·d), substantially reducing uncontrolled air exchange. In "Condition-Based Preservation" scenarios, the application of penetrating consolidates—though visually non-intrusive—effectively seals micro-cracks and pores, mitigating both air leakage and moisture penetration, thereby slowing thermal performance deterioration.

The efficacy of these interventions is quantitatively validated through standardized thermal performance metrics. Infrared thermography was conducted using a FLIR E8 camera under controlled conditions (outdoor temperature: 5 °C; indoor temperature: 18 °C); results are presented in Table 6. The thermal images reveal that surface temperature differentials across representative repaired zones decreased from 3 to 5 °C pre-repair to <1.5 °C post-repair, indicating substantial mitigation of thermal bridging. Complementary blower-door–type airtightness tests demonstrate an average 25–35% reduction in air permeability per unit area, corresponding to an estimated 15–30% decrease in theoretical annual heating energy consumption. These findings confirm that precise identification and targeted remediation of thermally significant envelope defects can efficiently enhance the energy performance of existing buildings.

Table 6. Infrared Thermography Data Comparison of Airtightness Loss.

Case Location	Defect Type	Repair Measures	Temperature Difference (°C) Before Repair	Temperature Difference (°C) After Repair	Decline in Air Permeability (%)
Huai'an Ji qing Supermarket	Structural cracks + insulation layer damage	Epoxy grouting + elastic sealing + roof rework	4.8	1.2	32%
Nanjing Xian he Ming yuan	The sealant has aged and the hangers have rusted	Replace silicone sealant and seal the joints	2.1	1.0	15%
Department Building	Micro-cracks (Type X)	Penetrating protective agent coating	1.2	1.0	4%

5. Conclusions

This study proposes an integrated technical framework—"intelligent defect detection, quantitative damage assessment, graded repair"—for managing envelope pathologies in modern civil buildings. A regional crack detection model and single-crack recognition/calibration model were successfully developed and optimized. Critically, the framework incorporates thermal performance evaluation: cracks were quantified to contribute 15–40% to total heat loss via thermal bridging and air leakage, and 20–40% to excess energy consumption through insulation moisture damage. Accordingly, repair strategies prioritize high-energy-risk cracks, employing elastic sealants or structural reinforcement to restore airtightness—projected to reduce HVAC loads by 15–30%. It should be emphasized that the energy-efficiency-prioritized retrofitting strategy proposed in this study is applicable only to existing buildings whose building envelopes remain largely intact, with defects that are localized and manageable. In cases where buildings exhibit extensive facade spalling, structural cracking, severe moisture intrusion, or other forms of irreversible deterioration, localized energy-efficiency interventions are neither cost-effective nor technically viable; under such circumstances, the feasibility of demolition and reconstruction should be prioritized for evaluation. To address this, we have incorporated an initial screening stage at the front end of the proposed methodology. This triage step assesses three key criteria—structural safety, remaining service life of primary building components, and the proportion of retrofitting costs relative to total rehabilitation expenditure—to determine the suitability of applying the proposed approach.

By tailoring repair approaches to material-specific defects (brick-concrete, dry-hung stone, true-stone paint) and emphasizing "aesthetic integration," the methodology ensures both structural safety and energy efficiency—avoiding new thermal bridges through low-conductivity sealants. Although the proposed framework demonstrates considerable potential for energy-oriented building envelope repair within the context of this study, its current implementation is still based on regional datasets. To achieve broader applicability, the model needs to be retrained and calibrated using diverse datasets that reflect global architectural traditions, material properties, and climate-induced damage patterns. Therefore, we position this study as a fundamental step toward scalable AI-aided building diagnosis rather than a fully refined universal solution.

Future work will expand the training dataset to encompass diverse structural typologies and integrate key thermal metrics (air permeability, thermal bridge intensity) into the assessment pipeline, advancing repair strategies from structural safety toward whole-life-cycle energy optimization. Future work will directly incorporate probabilistic outputs into the grading framework, thereby enabling risk-oriented maintenance decisions that explicitly account for detection confidence levels. Furthermore, integration with Building Information Modeling (BIM) and digital twin technology—featuring 3D pathology modeling and thermal simulation—will enable dynamic, data-driven conservation management. Ultimately, this research pioneers the convergence of artificial intelligence and architectural conservation, transforming building envelopes from passive safety barriers into active components of near-zero-energy building systems.

Author Contributions: Conceptualization, D.L., T.Z., W.Z. and Q.N.; methodology, D.L.,T.Z. and W.Z.; software, D.L. and T.Z.; validation, D.L. and T.Z.; formal analysis, T.Z. and Q.N.; investigation, D.L. and T.Z.; resources, D.L. and T.Z.; data curation, T.Z. and W.Z.; writing—original draft preparation, D.L. and T.Z.; writing—review and editing, D.L. and T.Z.; visualization, D.L. and T.Z.; supervision, D.L. and W.Z.; project administration, D.L. and T.Z.; funding acquisition, D.L. and T.Z. All authors have read and agreed to the published version of the manuscript.

Funding: This research was funded by the Postgraduate Research & Practice Innovation Program of Suzhou University of Science and Technology (SJCX24_1858) and Jiangsu Provincial Engineering Research Center for Building Carbon Neutrality Technology, Suzhou University of Science and Technology and the National Natural Science Foundation of China (No. 51908393) and the National Natural Science Foundation of China (Grant No. 52508006) and the Open Foundation of Anhui Province Key Laboratory of Intelligent Building and Building Energy Saving (No. IBES2025KF07).

Data Availability Statement: All data are available from the corresponding author by request.

Conflicts of Interest: The authors declare no conflicts of interest.

References

1. Karimi, N.; Mishra, M.; Lourenço, P.B. Deep learning-based automated tile defect detection system for Portuguese cultural heritage buildings. *J. Cult. Herit.* **2024**, *68*, 86–98. [CrossRef]
2. Lakatos, Á. Novel Thermal Insulation Materials for Buildings. *Energies* **2022**, *15*, 6713. [CrossRef]
3. Yadav, D.P.; Kishore, K.; Gaur, A.; Kumar, A.; Singh, K.U.; Singh, T.; Swarup, C. A Novel Multi-Scale Feature Fusion-Based 3SCNet for Building Crack Detection. *Sustainability* **2022**, *14*, 16179. [CrossRef]
4. Jroundi, F.; Priego, P.C.; Merroun, L.M.; González Muñoz, M.T.; Rodríguez Navarro, C.M. Insights into the influence of reinforcing iron bars corrosion on historical buildings: Towards optimizing limestone performance. *J. Build. Eng.* **2025**, *111*, 113203. [CrossRef]
5. Gil-Martín, L.M.; Hdz-Gil, L.; Kohrangi, M.; Menéndez, E.; Hernández-Montes, E. Fragility curves for historical structures with degradation factors obtained from 3d photogrammetry. *Heritage* **2022**, *4*, 3260–3279. [CrossRef]
6. Kumar, A.; Singh, V.P.; Dutt, N. *Thermal Energy Systems: Design, Computational Techniques, and Applications*; CRC Press: Boca Raton, FL, USA, 2023; pp. 32–37.
7. Li, L.; Chen, B.; Zhou, L.; Xia, Q.; Zhou, Y.; Zhou, X.; Xia, Y. Thermal behaviors of bridges—A literature review. *Adv. Struct. Eng.* **2023**, *26*, 985–1010. [CrossRef]
8. Kempton, L.; Daly, D.; Kokogiannakis, G.; Dewsbury, M. A rapid review of the impact of increasing airtightness on indoor air quality. *J. Build. Eng.* **2022**, *57*, 104798. [CrossRef]
9. Liu, T.; Chen, L.; Yang, M.; Sandanayake, M.; Miao, P.; Shi, Y. Sustainability considerations of green buildings: A detailed overview on current advancements and future considerations. *Sustainability* **2022**, *14*, 14393. [CrossRef]
10. Dong, Q.; Ma, C.; Zhang, R.; Hu, B.; Tian, C.; Li, M.; Sun, X. 3D mound information perception for construction sites based on binocular vision. In Proceedings of the 2nd International Conference on Information Technology and Intelligent Control (CITIC 2022), Kunming, China, 15–17 July 2022; Volume 12346, pp. 206–211.
11. Ma, L.; Xu, H.; Zhao, S.; He, J.; Tian, Y.; Yu, Z. Hollowing defect detection and risk assessment of facade tile shedding in high-rise residential buildings using the UAV–mounted infrared thermography method. *J. Build. Eng.* **2025**, *113*, 113840. [CrossRef]
12. Caspani, V.F.; Tonelli, D.; Poli, F.; Zonta, D. Designing a Structural Health Monitoring System Accounting for Temperature Compensation. *Infrastructures* **2022**, *7*, 5. [CrossRef]
13. Ruzek, P.; Kadlec, M.; Tserpes, K.; Karachalios, E. Monitoring of compressive behaviour of stiffened composite panels using embedded fibre optic and strain gauge sensors. *Int. J. Struct. Integr.* **2017**, *8*, 134–150. [CrossRef]
14. Curran, P.; Tilly, G. Design and monitoring of the Flintshire Bridge, UK. *Struct. Eng. Int.* **1999**, *9*, 225–228. [CrossRef]
15. Mufti, A.A.; Neale, K.W. State-of-the-art of FRP and SHM applications in bridge structures in Canada. *Compos. Polycon* **2007**, *2*, 60–69.
16. Li, S.; Wu, Z.; Zhou, L. Health monitoring of flexural steel structures based on distributed fibre optic sensors. *Struct. Infrastruct. Eng.* **2010**, *6*, 303–315. [CrossRef]
17. Navarro, V.; Moya, M.; Asensio, L.; Alonso, J. Underwater monitoring of the cracks found in Santos Morcillo Lake, Central Spain. *Geotech. Test. J.* **2013**, *36*, 163–168. [CrossRef]
18. Li, H.; Kang, L.; Sun, H.; Wu, J.; Zhao, Y.; Amihere, S. Fixed Automated stations location and UAVs routing problems in urban road Networks: A tailored Branch-&-price algorithm. *Transp. Res. A-Pol. Pract.* **2024**, *189*, 104–201.
19. Akyürek, A.H.; Kozan, I.H.; Taşdemir, Ş. Surface Crack Detection in Historical Buildings with Deep Learning-based YOLO Algorithms: A Comparative Study. *Comput. Res. Prog. Appl. Sci. Eng.* **2025**, *10*, 1–14. [CrossRef]
20. Czyża, S.; Szuniewicz, K.; Kowalczyk, K.; Dumalski, A.; Ogrodniczak, M.; Zieleniewicz, Ł. Assessment of accuracy in unmanned aerial vehicle (uav) pose estimation with the real-time kinematic (rtk) method on the example of dji matrice 300 rtk. *Sensors* **2023**, *23*, 2092. [CrossRef]
21. Gordan, M.; Razak, H.A.; Ismail, Z.; Ghaedi, K.; Tan, Z.X.; Ghayeb, H.H. A hybrid ANN-based imperial competitive algorithm methodology for structural damage identification of slab-on-girder bridge using data mining. *Appl. Soft Comput.* **2020**, *88*, 106013. [CrossRef]

22. Martin, M.; Chong, A.; Biljecki, F.; Miller, C. Infrared thermography in the built environment: A multi-scale review. *Renew. Sust. Energ. Rev.* **2022**, *165*, 112540. [CrossRef]
23. Inazumi, S.; Shakya, S.; Komaki, T.; Nakanishi, Y. Numerical Analysis on Performance of the Middle-Pressure Jet Grouting Method for Ground Improvement. *Geosciences* **2021**, *11*, 313. [CrossRef]
24. Lauermannová, A.-M.; Paterová, I.; Patera, J.; Skrbek, K.; Jankovský, O.; Bartůněk, V. Hydrotalcites in Construction Materials. *Appl. Sci.* **2020**, *10*, 7989. [CrossRef]
25. Thansirichaisree, P.; Ejaz, A.; Saingam, P.; Mohamad, H.; Hussain, Q.; Chaimahawan, P.; Bhadrakom, B.; Buddhawanna, S. Green reinforcement techniques: Using natural hemp and cotton ropes to enhance the structural integrity of short-span RC beams. *J. Infrastruct. Intell. Resil.* **2025**, *4*, 100168. [CrossRef]
26. Ghasemi, S.; Mirmiran, A.; Xiao, Y.; Mackie, K. Novel UHPC-CFRP Waffle Deck Panel System for Accelerated Bridge Construction. *J. Compos. Constr.* **2016**, *20*, 04015042. [CrossRef]
27. Moujalled, B.; Leprince, V.; Berthault, S.; Litvak, A.; Hurel, N. Mid-term and long-term changes in building airtightness: A field study on low-energy houses. *Energy Build.* **2021**, *250*, 111257. [CrossRef]
28. Becoche Mosquera, J.M.; Macías Pinto, D.J. Global Perspectives on Riparian Ecosystem Restoration: A Systematic Literature Review. *World* **2025**, *6*, 164. [CrossRef]
29. Morfoulaki, M.; Chatziathanasiou, M.; Anapali, I.S. Social Planning for eBRT Innovations: Multi-Criteria Evaluation of Societal Impacts. *World Electr. Veh. J.* **2025**, *16*, 661. [CrossRef]
30. Camblong, H.; Zapirain, I.; Curea, O.; Ugartemendia, J.; Boussaada, Z.; Zamora, R. Rule-Based Energy Management System to Enhance PV Self-Consumption in a Building: A Real Case. *Energies* **2024**, *17*, 6099. [CrossRef]
31. De Medici, S.; Cataldi, G.; Costanzo, V.; Vitale, M.R. Balancing Cultural Values and Energy Transition: A Multi-Criteria Approach Inspired by the New European Bauhaus. *Sustainability* **2025**, *17*, 11255. [CrossRef]
32. Khanam, R.; Hussain, M. Yolov11: An overview of the key architectural enhancements. *arXiv* **2024**, arXiv:2410.17725. [CrossRef]
33. Zhao, Q.; Zhu, J. An Improved YOLOv11 architecture with multi-scale attention and spatial fusion for fine-grained residual detection. *Results Eng.* **2025**, *27*, 107061. [CrossRef]
34. Deng, C.; Wu, Y.; Wu, Z.; Zhou, W.; Zhang, Y.; Sun, X.; Wang, S. YOLO-AEB: PCB Surface Defect Detection Based on Adaptive Multi-Branch Attention and Efficient Atrous Spatial Pyramid Pooling. *Computers* **2025**, *14*, 543. [CrossRef]
35. Rani, U.M.; Rajesh, A.; Rao, V.V.; Prasanna, K.L.; Vasanthi, P. Extreme small object detection with transformer-based local and global context attention. *Infrared Phys. Technol.* **2025**, *152*, 106251. [CrossRef]
36. Gu, X.; Liu, M.; Tian, J. State of Health Estimation for Batteries Based on a Dynamic Graph Pruning Neural Network with a Self-Attention Mechanism. *Energies* **2025**, *18*, 5333. [CrossRef]
37. Di Ludovico, M.; De Martino, G.; Manfredi, V.; Masi, A.; Prota, A.; Sorrentino, L.; Zucconi, M. Loss Functions for the Risk Assessment of Residential Buildings. *Buildings* **2023**, *13*, 2817. [CrossRef]
38. Han, K.; Xiao, A.; Wu, E.; Guo, J.; Xu, C.; Wang, Y. Transformer in transformer. *Adv. Neural Inf. Process. Syst.* **2021**, *34*, 15908–15919.
39. Fitsum, T.; Yina, S.; Sudhakar, M. Thermal performance of flat roof insulation materials: A review of temperature, moisture and aging effects. *J. Build. Eng.* **2023**, *76*, 107142. [CrossRef]
40. Mohammadi, M.; Atsbha, T.G.; Chen, Y. Comparison and Design of Dry-Stack Blocks with High Thermal Resistance for Exterior Walls of Sustainable Buildings in Cold Climates. *Sustainability* **2025**, *17*, 1393. [CrossRef]
41. Jezierski, W.; Szczepaniak, P.; Leszczyński, C. Optimization of Thermal Insulation Parameters for Vertical Perimeters in Buildings with Single-Layer Walls. *Buildings* **2025**, *15*, 405. [CrossRef]
42. Vargova, A.; Köhler, S.; Hötzel, S.; Schröter, B.; Vranayova, Z.; Kaposztasova, D. Transformation of Urban Spaces: The Impact of Green Roofs in Košice, Slovakia. *Sustainability* **2024**, *16*, 22. [CrossRef]

Disclaimer/Publisher's Note: The statements, opinions and data contained in all publications are solely those of the individual author(s) and contributor(s) and not of MDPI and/or the editor(s). MDPI and/or the editor(s) disclaim responsibility for any injury to people or property resulting from any ideas, methods, instructions or products referred to in the content.